

See discussions, stats, and author profiles for this publication at: <https://www.researchgate.net/publication/231654881>

Oxidation State and Local Structure of Ti-Based Additives in the Reactive Hydride Composite $2\text{LiBH}_4 + \text{MgH}_2$

ARTICLE in THE JOURNAL OF PHYSICAL CHEMISTRY C · JANUARY 2010

Impact Factor: 4.77 · DOI: 10.1021/jp910955r

CITATIONS

44

READS

37

10 AUTHORS, INCLUDING:



Francisco Javier Palomares

Spanish National Research Council

133 PUBLICATIONS 1,216 CITATIONS

[SEE PROFILE](#)



Christian Bonatto Minella

Karlsruhe Institute of Technology

31 PUBLICATIONS 443 CITATIONS

[SEE PROFILE](#)



M. Dornheim

Helmholtz-Zentrum Geesthacht

140 PUBLICATIONS 2,754 CITATIONS

[SEE PROFILE](#)



Asuncion Fernandez

Spanish National Research Council - Institut...

246 PUBLICATIONS 6,409 CITATIONS

[SEE PROFILE](#)

Oxidation State and Local Structure of Ti-Based Additives in the Reactive Hydride Composite $2\text{LiBH}_4 + \text{MgH}_2$

E. Deprez,[†] Miguel A. Muñoz-Márquez,[†] Manuel A. Roldán,[†] C. Prestipino,[‡]
 F. Javier Palomares,[§] C. Bonatto Minella,^{||} U. Bösenberg,^{||} M. Dornheim,^{||} R. Bormann,^{||} and
 A. Fernández^{*,†}

Instituto de Ciencia de Materiales de Sevilla, CSIC-Univ. Sevilla, Avenida Américo Vespucio 49, 41092 Seville, Spain, ESRF, 38043 Grenoble Cedex, France, Instituto de Ciencia de Materiales de Madrid, CSIC, Cantoblanco, 28049 Madrid, Spain, and Institute of Materials Research, GKSS Research Centre, Max-Planck-Str. 1, D-21502, Geesthacht, Germany

Received: November 18, 2009; Revised Manuscript Received: January 8, 2010

Nowadays, the technological utilization of reactive hydride composites (RHC) as hydrogen storage materials is limited by their reaction kinetics. However, addition of transition-metal-based additives, for instance titanium isopropoxide (Ti-iso), to the $2\text{LiBH}_4 + \text{MgH}_2$ system, results in a significant improvement of sorption kinetics. In this work, the evolution of chemical state and local structure of the Ti-based additive has been investigated by means of X-ray absorption (XAS) and photoemission (XPS) spectroscopy. X-ray absorption near-edge structure (XANES) as well as extended X-ray absorption fine structure (EXAFS) analysis have been undertaken at the Ti K-edge. The measurements reveal the formation of a highly dispersed and disordered TiO_2 -like phase during ball milling. During first desorption reduced titanium oxide and titanium boride are formed and remain stable upon cycling. The surface analysis performed by XPS shows that the reduction processes of the Ti-based additive during first desorption is coupled to the migration of the Ti species from the surface to the bulk of the material. Several factors, related to favoring heterogeneous nucleation of MgB_2 and the increase of interfacial area through grain refinement are proposed as potential driving force, among other effects, for the observed kinetic improvement.

Introduction

Considering the increase of the CO_2 emissions and the short-medium term exhaustion of fossil fuels, new energy concepts are essential for the future of industrial society. Hydrogen is one of the favored energy carriers for the future since it has the highest energetic power, it is a non polluting fuel and water is the only result of its combustion.^{1–3} However, the development of future mobile applications involves the necessity of finding a safe and efficient way of storing hydrogen. Promising materials are metal hydride systems; they permit to store hydrogen in the form of metal hydrides and have a high storage capacity per unit volume. Special attention has been paid on lightweight metal hydrides and complex hydrides,^{4–6} which offer a great volumetric hydrogen density and show reversible reactions.

Lithium borohydride, LiBH_4 is a very interesting material because of its high theoretical gravimetric capacity (about 18.5 wt %);^{7,8} however, it still suffers from slow reaction kinetics and high thermodynamic stability. Nevertheless improvement of the reaction rates is possible through destabilization of the complex hydride, for example, by coupling with a metal hydride. Recently, the addition of magnesium hydride, MgH_2 , has been proved to be a good destabilizing agent for LiBH_4 .^{9,10} The dehydrogenation of $2\text{LiBH}_4 + \text{MgH}_2$ occurs according to the reaction: $2\text{LiBH}_4 + \text{MgH}_2 \leftrightarrow 2\text{LiH} + \text{MgB}_2 + 4\text{H}_2$ which releases about 10.5 wt % of hydrogen, additionally the reaction

is found to be reversible. The formation of MgB_2 appears to stabilize the dehydrogenated state and therefore decreases the total reaction enthalpy of the system. The pure LiBH_4 has been shown to be reversible^{11–13} but at much higher temperature than the RHC.

Depending on pressure and temperature, the $2\text{LiBH}_4 + \text{MgH}_2$ reactive hydride composite (RHC) frequently shows a two-step desorption mechanism. First, MgH_2 desorbs and forms Mg; thereafter LiBH_4 decomposes forming LiH and MgB_2 whereby more hydrogen is released.^{14,15} The appearance of an incubation period between the two steps described by Bösenberg et al.¹⁴ makes the overall reaction very slow. However, kinetics could be enhanced by suitable additives, such as transition metal chlorides or oxides.^{14–17} Particularly, the metal organic compound Titanium isopropoxide (Ti-iso) has shown to significantly improve the kinetics of the $2\text{LiBH}_4 + \text{MgH}_2$ system and especially the desorption of LiBH_4 .¹⁴

So far the reaction mechanism and the influence of the Ti-iso additive are not yet fully understood. We have performed a full analysis of the surface, subsurface and bulk regions in order to investigate the oxidation state and the local structure of the additive. For this purpose, X-ray absorption spectroscopy (XAS) experiments studying the XANES (X-ray absorption near edge structure) and the EXAFS (extended X-ray absorption fine structure) regions, in combination with X-ray photoelectron spectroscopy (XPS) measurements have been performed to obtain information on the evolution of the Ti phases during the different steps of milling, desorption, and absorption of hydrogen. In previous papers, we have presented a pioneering work which demonstrates the usefulness of these X-ray based techniques to understand the role of Nb-based additives in

* To whom correspondence should be addressed. E-mail: asuncion@icmse.csic.es. Tel: +34 954 48 95 31. Fax: +34 954 46 06 65.

[†] Instituto de Ciencia de Materiales de Sevilla.

[‡] ESRF.

[§] Instituto de Ciencia de Materiales de Madrid.

^{||} Institute of Materials Research.

nanostructured MgH₂ for an efficient H₂ storage.^{18–20} Also very recently, several authors of the present work have also demonstrated the potential of the XAS technique, specifically the XANES region, to study the evolution of the chemical state of Zr-based additives in the RHC system 2LiBH₄ + MgH₂.²¹ Finally, it is worth mentioning the investigation carried out by Ignatov et al.²² where a complete study of the evolution of the TiCl₃ and NiCl₂ added to complex metal hydrides is presented. In the current research work, we present a comprehensive analysis of the role of the Ti-iso additive by using the XANES as well as the EXAFS regions of the absorption spectrum.

The present study provides pioneer results concerning the chemical state of the Ti-iso additive in the RHC systems as well as surface information which contribute to the understanding of the reaction mechanism and the influence of the additive on the kinetics. This work is of high interest since additives, as amorphous or nanostructured highly diluted phases, are playing a very important role in the kinetic improvement of the sorption reaction^{14,15} ad-hoc techniques are needed to characterize these phases. Transmission electron microscopy (TEM) and X-ray diffraction (XRD) analysis have been also carried out to determine the evolution of the RHC phases and to obtain alternative information on Ti-based phases when possible. Details of the TEM and XRD analysis will be reported in a separate paper.

Experimental Section

Sample Preparation. All samples were prepared by high energy ball milling in a Spex 8000 mixer mill using a ball (steel) to powder ratio of 10:1. The initial microcrystalline powders, LiBH₄ (95% purity), MgH₂ (98% purity, the rest being Mg) and Titanium isopropoxide (99.995% purity) were purchased from Alfa Aesar. The MgH₂ was premilled for 5 h before being mixed to LiBH₄ and 10 (or 5) mol % of Ti-iso for a further 5 h milling. A set of samples without additive was also prepared to be used as a reference.

To prepare the samples at the different sorption stages, hydrogen cycling was performed using a thermovolumetric Sieverts apparatus designed by Hydro Quebec/HERA Hydrogen Storage System. Desorption reactions were performed at 400 °C under 5 bar hydrogen, whereas the absorption reactions were measured at 350 °C under 50 bar hydrogen.

The samples were prepared and handled under continuously purified argon or nitrogen atmosphere in gloveboxes.

Spectroscopic Characterization. XAS measurements of samples with 10 mol % Ti-iso have been performed in transmission mode at BM29 beamline²³ at the European Synchrotron Radiation Facility (ESRF, Grenoble, France). The fixed exit monochromator was equipped with two Si(111) crystals and harmonic rejection was achieved by the use of Si double system mirror. Spectra have been collected at Ti K-edge in the energy ranges 4850–6200 eV under vacuum conditions at ambient temperature. Samples with 5 mol % Ti-iso were measured at beamline A1 (Hasylab, DESY) in Hamburg (Germany) in the same energy range at ambient temperature. The beamline is equipped with a Si(111) channel cut double crystal monochromator, and harmonic rejection was achieved by the use of a two mirror system (the first mirror is coated with Ni and the second mirror has two stripes one coated with Ni and the other one uncoated SiO₂).

The prepared and treated samples were mixed with boron nitride powder for dilution before XAS experiments. The resulting powders were placed between two Kapton foils on

aluminum sample holders, which could be sealed under Ar in a glovebox before the analysis.

TiB₂, Ti₂O₃, TiO₂ anatase, and TiO samples were purchased from Sigma Aldrich, to be used as a reference for XAS measurements.

EXAFS and XANES data processing has been carried out by the software ATHENA and ARTHEMIS²⁴ two interactive graphical utility based on the IFFEFIT²⁵ library of numerical and XAS algorithms. XANES data analysis has been performed subtracting the pre-edge background and normalizing the edge jump to one.

The obtained EXAFS spectra were analyzed by the nonlinear least-squares fit algorithm implemented in ARTHEMIS software using the phase shift $\phi_j(k)$ and backscattering amplitude functions, $F_j(k)$, calculated with the FEFF 6 L²⁶ code. To fit the spectra, the single scattering paths (SS) corresponding to each coordination shell were used.

For each coordination shell, the coordination number (N), bond distance (R), and Debye–Waller factor (σ) were extracted.

XPS spectra were recorded with a SPECS Phoibos150 electron spectrometer and a Delay Line Detector in the 9 segmented mode, using Al K α radiation (1486.6 eV) in an ultrahigh vacuum chamber at a base pressure of 6×10^{-10} mbar. Ti 2p core level XPS spectra were acquired with 20 eV pass energy and 0.5 eV energy step at normal emission takeoff angle. The binding energy reference was taken as the main component of the C1s peak at 284.6 eV for a mixture of adventitious carbon.

The 5 mol % additives samples were deposited onto adhesive Cu substrates inside the glovebox and transported in N₂ atmosphere to the XPS spectrometer. A portable glovebox is coupled to the XPS load-lock chamber so samples can be introduced without being exposed to air.

TEM and XRD Investigations. TEM analysis was performed in a Philips CM200 microscope operating at 200 kV and equipped with an energy-dispersive X-ray (EDX) detector. Samples were diluted into toluene inside the glovebox, dropped onto a copper grid and introduced into the microscope. A vacuum gate valve allowed the sample to be isolated in a prechamber for complete evaporation of toluene prior to transfer for analysis.

XRD measurements were performed with a powder diffractometer Siemens D5000-D with a goniometer for transmission geometry and carried out with Cu K α radiation. The samples were sealed in a glass capillary inside the glovebox. Data acquisition was performed for 2θ angle range of 20–90°.

Results and Discussion

Description of Samples under Investigation. Figure 1 shows a preliminary microstructural and compositional analysis, as obtained by TEM/EDX, for the original milled 2LiBH₄ + MgH₂ sample with (b) and without (a) the Ti-iso additive and a pure LiBH₄ milled sample (c) for comparison purposes. Particles with sizes in the range 0.1–1 μ m appear in the micrographs with a darker contrast and are identified by EDX as the MgH₂ particles. These particles are polycrystalline and can evolve to Mg by electron irradiation. In addition, a lighter matrix appears surrounding the MgH₂ particles. These areas have been identified as the LiBH₄ phase, as determined by EDX by comparison to a pure LiBH₄ sample. The Ti-based additive has been detected by EDX in the corresponding sample (b). The analysis in different regions shows a uniform distribution of titanium in the sample down to an observed size scale of approximately 100 nm. The data indicate a very fine additive distribution and sizes much smaller than 100 nm for the corresponding additive

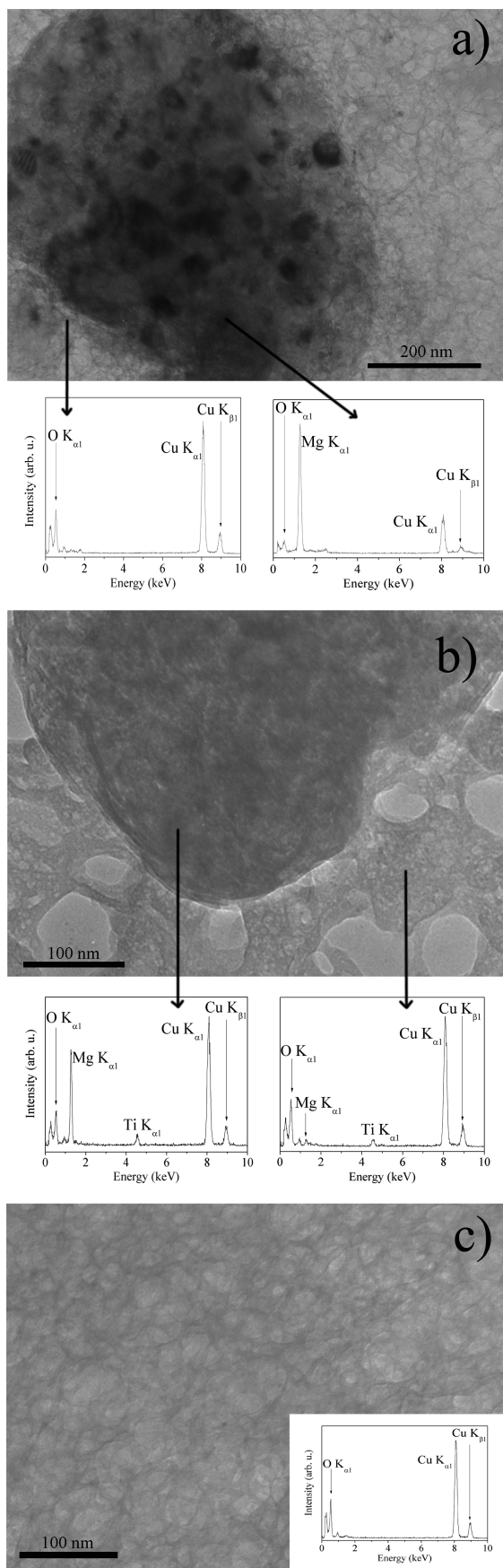


Figure 1. TEM micrographs and EDX spectra from representative areas (as indicated by the arrows) for the following milled samples: (a) 2LiBH₄ + MgH₂, (b) 2LiBH₄ + MgH₂ + 5 mol % Ti-iso, and (c) pure LiBH₄.

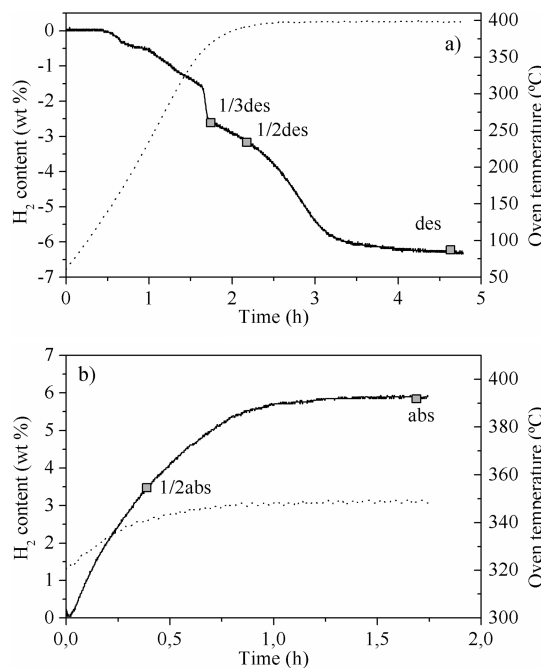
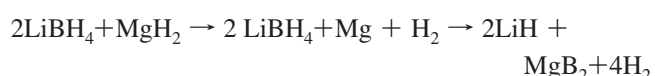


Figure 2. Desorption (a) and absorption (b) kinetic curves (solid line) of 2LiBH₄ + MgH₂ + 10 mol % Ti-iso. The oven temperature as a function of time is included (dashed line), the temperature is reflected in the left axis.

phase. A more detailed TEM analysis will be the subject of a further study.

For the experimental desorption temperatures of 400 °C and 5 bar hydrogen, i.e., below the equilibrium temperature of LiBH₄ at this pressure, the formation of MgB₂ is suggested to take place simultaneously to the desorption of LiBH₄.^{14,15} The desorption reaction proceeds under the aforementioned conditions in two steps:^{14,15}



Consequently, the reaction enthalpy is effectively lowered with respect to desorption of pure LiBH₄. Formation of MgB₂ upon desorption was observed to be a key factor for reversibility^{14,15} at temperatures lower than the desorption temperature of pure LiBH₄. Rehydrogenation to LiBH₄ under moderate temperatures and hydrogen pressure is only possible if the desorption products were LiH and MgB₂, and the reabsorption process occurs in one single step. An incubation period frequently occurs between the two desorption steps which, however, can be substantially reduced by the addition of transition metal compounds.¹⁴

Figure 2, shows the kinetic behavior of the desorption and absorption reactions of the reactive hydride composite 2LiBH₄ + MgH₂ + 10 mol % Ti-iso as prepared by high energy ball milling. In order to better understand the role and evolution of the Ti-additives during the ongoing sorption reactions, partially desorbed and partially absorbed samples have been prepared additionally to the conventional fully desorbed and absorbed samples. The 1/3 desorbed sample corresponds to the sample after the MgH₂ desorption, the 1/2 desorbed to the sample after the beginning of the LiBH₄ decomposition and the 1/2 absorbed to the materials with a half hydrogen content absorbed. It is important to note that the incubation period between the two steps of MgH₂ and LiBH₄ desorption is almost absent due to the addition of the

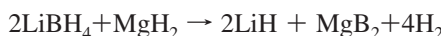
TABLE 1: Summary of investigated samples and labels

label	samples	condition
M10-org	2LiBH ₄ + MgH ₂ + 10 mol % Ti-iso. milled	after ball miling
M10-1/3Des	2LiBH ₄ + MgH ₂ + 10 mol % Ti-iso. + 1/3Des	after MgH ₂ desorption
M10-1/2Des	2LiBH ₄ + MgH ₂ + 10 mol % Ti-iso. + 1/2Des	after beginning of LiBH ₄ desorption
M10-Des	2LiBH ₄ + MgH ₂ + 10 mol % Ti-iso. + Des	after full desorption
M10-1/2Abs	2LiBH ₄ + MgH ₂ + 10 mol % Ti-iso. + 1/2Abs	after full desorption and half wt % hydrogen absorption
M10-Abs	2LiBH ₄ + MgH ₂ + 10 mol % Ti-iso. + Abs	after full desorption and full absorption
M5-org	2LiBH ₄ + MgH ₂ + 5 mol % Ti-iso. milled	after ball miling
M5-1/3Des	2LiBH ₄ + MgH ₂ + 5 mol % Ti-iso. + 1/3Des	after MgH ₂ desorption
M5-1/2Des	2LiBH ₄ + MgH ₂ + 5 mol % Ti-iso. + 1/2Des	after beginning of LiBH ₄ desorption
M5-Des	2LiBH ₄ + MgH ₂ + 5 mol % Ti-iso. + Des	after full desorption
M5-1/2Abs	2LiBH ₄ + MgH ₂ + 5 mol % Ti-iso. + 1/2Abs	after full desorption and half wt % hydrogen absorption
M5-Abs	2LiBH ₄ + MgH ₂ + 5 mol % Ti-iso. + Abs	after full desorption and full absorption

Ti-iso. In the case of absorption, a one step reaction is observed, and a kinetic improvement is obtained with respect to the composite without additive.

The prepared samples according to Figure 2 have been summarized in Table 1, as well as the abbreviated labels used throughout the paper. Similarly, samples have also been prepared with 5 mol % Ti-iso and their corresponding labels are also included in Table 1.

XRD have been used routinely to check the evolution of desorption and absorption reactions according to:



LiH, MgB₂, LiBH₄, and MgH₂ have been respectively identified as products of desorption and absorption reactions. However no Ti-based compound could be detected probably due to the amorphous and/or highly dispersed state of the Ti species. Therefore some other techniques like XAS and XPS are applied to obtain information on chemical state and local structure for the Ti containing phase.

X-ray Absorption Spectroscopy (XAS). XANES data measured at the Ti K-edge for milled and cycled samples are presented in Figure 3. The data of the as prepared milled samples are represented together with data for samples partially and fully desorbed and partially and fully absorbed after the first desorption. Parts a and b in the figure correspond to samples with 5 mol % Ti-iso and 10 mol % Ti-iso, respectively. The results reveal that irreversible changes in the oxidation state and local structure of the titanium additive occurs during the initial stages of the first desorption by heating at 400 °C under 5 bar H₂ pressure. The comparison of the M10-org, M10-1/3des and M10-1/2des samples (as representative of treated materials) with the reference compounds (Ti-iso, TiO₂, Ti, TiO, Ti₂O₃, and TiB₂) is shown in Figure 4.

The spectrum of the milled sample presents a first pre-edge at 4970 eV and comparable total edge absorption position to the fully oxidized Ti(IV). Taking into account the reaction of Ti-iso with traces of water resulting in titanium oxide,²⁷ the formation of TiO₂-like amorphous species during the milling process is likely to be considered. A very similar spectrum was obtained by dispersion of pure Ti-iso in BN powder (Ti-iso reference sample). It has been experimentally observed that as soon as a drop of the titanium isopropoxide is left to dry into the glovebox, a white powder appears indicating that, even under these anaerobic conditions, the hydrolysis of Ti-iso. is taking place. Additional sources of OH⁻ groups are highly reactive surfaces of MgH₂ and LiBH₄. Hydrolysis is therefore proposed here as the main primary process for decomposition of Ti-iso. leading to TiO₂-like species. The release of isopropanol can be

an additional source of carbon into the sample that will be discussed below.

A significant shift to lower energy is observed for the partially desorbed sample. Additionally the pre-edge observed with the

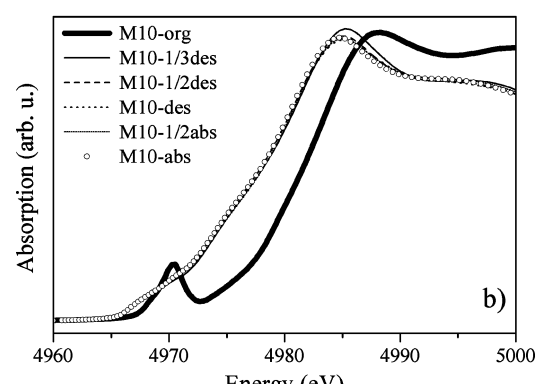
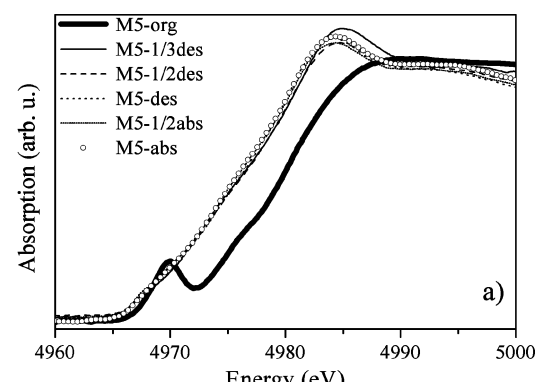


Figure 3. XANES data at the Ti K-edge for milled and cycled samples with 5 mol % Ti-iso (a) and 10 mol % Ti-iso (b).

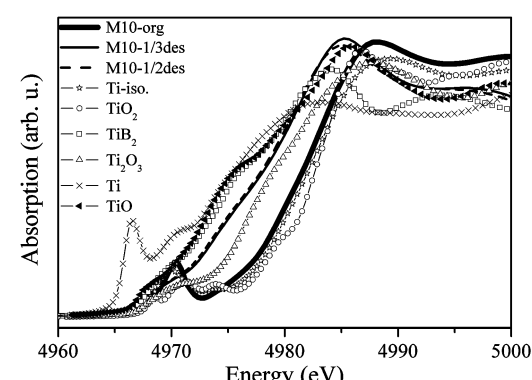


Figure 4. XANES data at the Ti K-edge for milled and desorbed samples (with 10 mol % Ti-iso) as compared to reference materials.

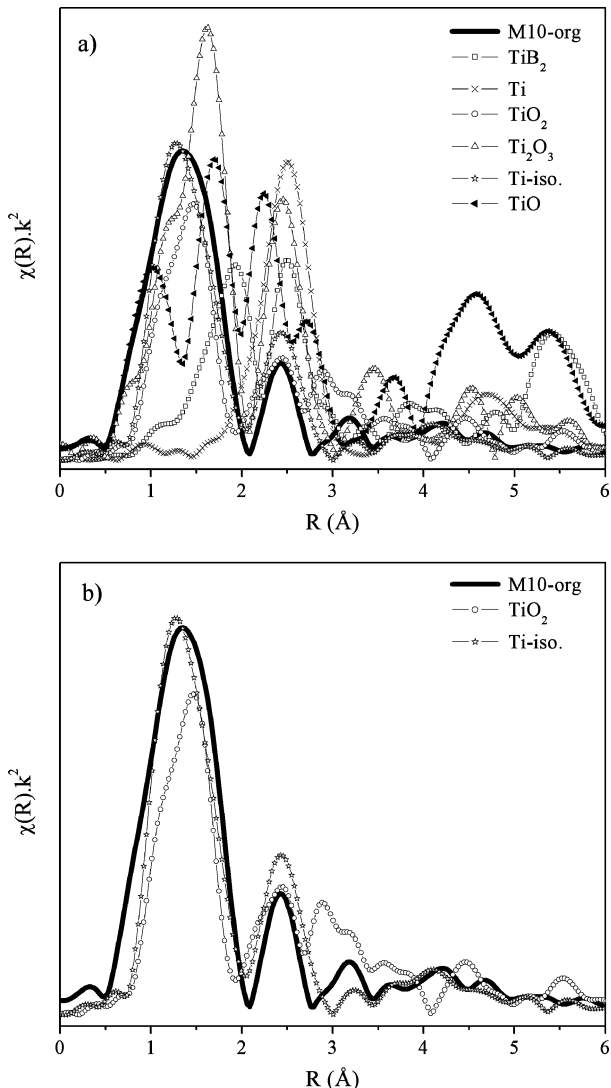


Figure 5. Fourier transform curves of the EXAFS oscillations: (a) As prepared M10-org milled material compared to all investigated references. (b) For clarity sake, only the M10-org sample compared to TiO₂ anatase and Ti-iso references are shown.

original milled material is strongly decreased. The Ti species are apparently reduced upon heating although the metallic Ti phase is not reached since the absorption edge is in an intermediate state between the Ti(II) (TiB₂ or TiO) and the Ti(III) (Ti₂O₃) oxidation states. This can be explained either by an unknown phase or a mixture of different chemical states of Ti after cycling. The EXAFS analysis (see below) will further support the latter hypothesis. Similar effects have been previously described²¹ for the ZrCl₄ and Zr-iso (Zr isopropoxide isopropanol complex) additives, where the edge position of the cycled materials for the Zr K-edge has reached the typical value of ZrB₂. It is worth to remark that no EXAFS data were presented in these previous studies hence, the added value of the current work.

Figures 5 and 6 present the Fourier transform (FT) curves of the EXAFS spectra for the milled and cycled materials as well as for the reference samples namely Ti metal, Ti-iso, different Ti-oxides, and Ti-boride. In Figure 5a the FT curve of the EXAFS spectrum from the as prepared M10-org milled material is compared with the corresponding spectra from all investigated references (Ti, TiO, Ti₂O₃, TiO₂, TiB₂, and Ti-iso). In Figure 5b only similar spectra are shown, the FT curve of the EXAFS spectrum from the M10-org sample which looks quite similar

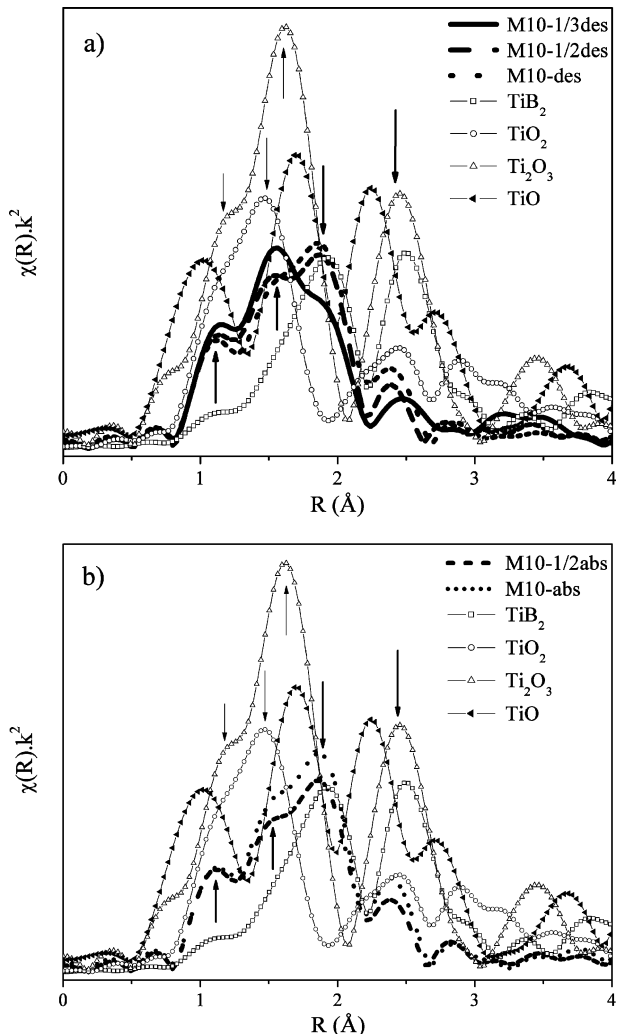


Figure 6. Fourier transform curves of the EXAFS oscillations: (a) Partially and fully desorbed samples and (b) partially and fully absorbed (after first desorption) samples. For 2LiBH₄ + MgH₂ + 10 mol % Ti-iso as compared to indicated reference materials.

to the curve obtained from the spectrum of TiO₂ anatase reference sample; although the closest resemblance is found with the data from the Ti-iso reference sample which was obtained by the mixture of Ti-iso and BN powder. Typical Ti–O bonds appear in a first coordination shell around 1.4 Å (without phase shift correction). Also Ti–Ti bonds are measured in the second coordination shell at 2.5 Å (also without phase shift correction). Fitting analysis will be shown below. The qualitative observed differences between the TiO₂ reference and the other two samples in Figure 5b are the ones expected for the formation of TiO₂ anatase like phase (with high degree of disorder or nanocrystalline) as the direct product of the hydrolysis of Ti-isopropoxide. The absence of long-range order, as compared to the polycrystalline TiO₂ reference material, is also a typical behavior of hydrolysis products from Ti-isopropoxide.

The FT data for the partially and fully desorbed M10 samples are represented in Figure 6a in comparison to relevant references. The reduction process from fully oxidized Ti(IV) in the M10-org as observed in the XANES region (Figure 3) can be also detected in the EXAFS data. In the case of FT data it is also possible to observe differences between 1/3, 1/2 and fully desorbed samples. All desorbed samples show three peaks in the 0.5 to 2.2 Å region. The two first, located at around 1.15 Å and 1.55 Å (without phase shift corrections), correspond to

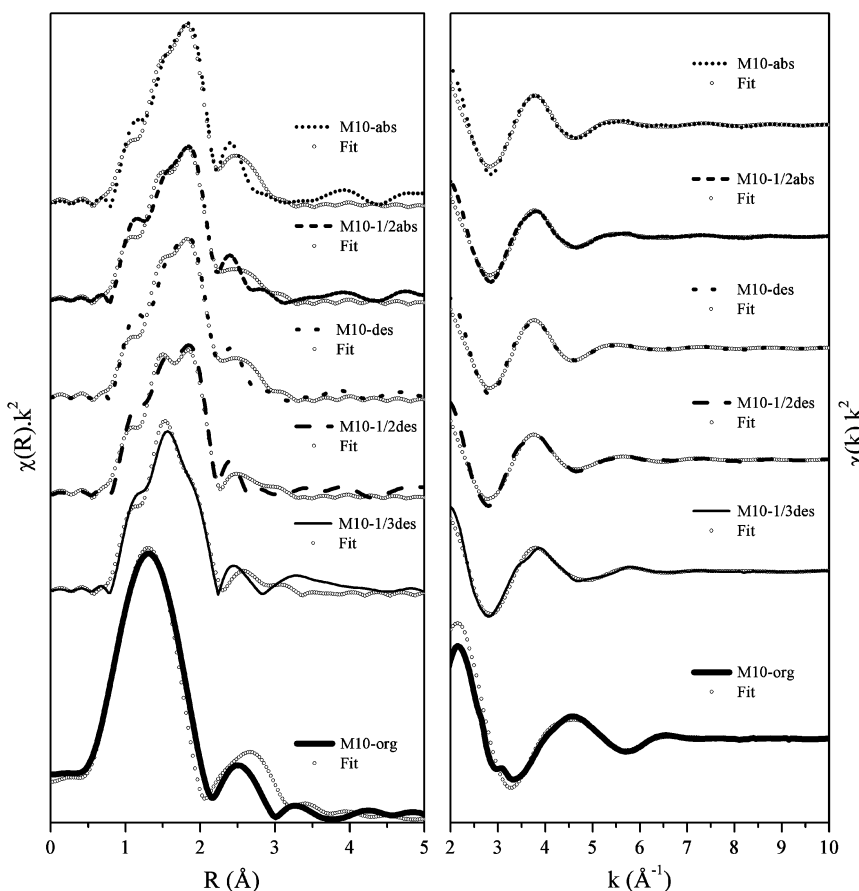


Figure 7. Experimental and best fit k^2 -weighted EXAFS for samples M10-org, M10-1/3des, M10-1/2des, M10-des, M10-1/2abs, and M10-abs.

Ti–O bond distances in the first coordination shell of the Ti_2O_3 reference material. The intensity of these two peaks decreases progressively during first desorption indicating a further reduction process. The third peak located at 1.9 Å (without phase shift correction), corresponds to Ti–B distances in the first coordination shell of TiB_2 and is progressively increasing across this process. We therefore propose that the evolution of the Ti-iso additive during desorption is leading to a final state which is mainly a mixture of Ti(III) as Ti_2O_3 and Ti(II) as TiB_2 . The remaining of a TiO_2 like phase cannot be fully disregarded by the current data. It is also worth of mention that another peak at around 2.4 Å (no phase shift correction) is detected, were contributions for Ti–Ti bonds in both TiB_2 and Ti_2O_3 are expected. The intensity of these peaks are smaller for milled and cycled samples indicating a high dispersion/amorphicity of the Ti phases and a certain degree of disarrangements of the local structure as compared to crystalline reference samples. The formation of isopropanol during hydrolysis of the additives can be also source of carbon in the sample. However, the formation of TiC species is expected to occur at much higher temperatures²⁸ than the ones used in this work. Additionally the XANES and EXAFS spectra at the Ti K-edge mainly fit with the reported data for Ti_2O_3 and TiB_2 .

The results described above are crucial for the understanding of the role of Ti additives to improve the kinetic behavior of the $2\text{LiBH}_4 + \text{MgH}_2$ RHC system. It is proposed here that stable TiB_2 species are formed which can favor the nucleation of MgB_2 and therefore improve the kinetic of the desorption reaction. A similar mechanism has been proposed for the Zr-based additives with formation of ZrB_2 .²¹ In particular, the reduction of the incubation period between the two desorption steps is striking. In an earlier study, a nucleation problem of MgB_2 was proposed

to be the origin of the incubation period.¹⁴ Lattice misfits are important factors for heterogeneous nucleation. Calculated lattice misfit between the {0001} basal-plane of MgB_2 and the {0001} basal-plane of TiB_2 is 1.8% (even smaller than for ZrB_2 for example). Therefore the observed TiB_2 might act as a nucleation agent for MgB_2 .

Furthermore, borides, especially TiB_2 , are known as outstanding grain refiners in Mg and Al alloys^{29,30} this effect will conduct also to kinetic improvements by increasing the presence of surfaces/interfaces for reactions. Although the LiBH_4 phase is melting at operating temperatures, both desorption and absorption processes in the RHC system occur at liquid–solid interface due to the presence of solid Mg, LiH, and MgB_2 phases.

In Figure 6b the FT data are represented for the partially and fully absorbed samples obtained after first desorption. Curves are similar to the ones obtained for the fully desorbed sample. In agreement with XANES data, once the active species are formed during first desorption, the oxidation state and local structure of the Ti-based additive remains almost constant. The H_2 absorption process after the first desorption is a one step process (see Figure 2), which kinetics is also favorably improved by the presence of the Ti-based additive. Similar species, as the ones (Ti-boride and Ti-oxide) identified after the first desorption were found after reabsorption. Moreover, grain refinement due to the enhanced nucleation frequency during desorption is proposed to increase the interfacial area, which results in a kinetic improvement also for absorption.

In order to quantify, at least in a semiquantitative way, the data shown in Figures 5 and 6, the fitting of EXAFS oscillations was undertaken for reference samples and RHC samples in the 0.50 to 3.00 Å range. Due to the data quality the k range for data analysis was 2.5–11.0 Å⁻¹ which is somewhat shorter than expected

TABLE 2: EXAFS Fitting Parameters^a of TiO₂ Anatase (Reference), Ti-iso. (Reference), and M10-org Samples

	shell	<i>N</i>	<i>R</i> (Å)	ΔE (eV)	σ (Å)	<i>R</i> factor
TiO ₂ anatase (tetragonal, I41/amd $a = 3.785 \text{ \AA}$, $c = 9.514 \text{ \AA}$)	O	4	1.94			
	O	2	1.97			
	Ti	4	3.01			
TiO ₂ anatase reference	O	4	1.89	-10.00	0.003	0.141
	O	2	1.98		0.008	
	Ti	4	3.03		0.010	
M10-org	O	4	1.91	-3.27	0.010	0.044
	O	2	2.05		0.015	
	Ti	4	3.10		0.026	
Ti-iso. reference	O	4	1.84	-15.00	0.009	0.064
	O	2	1.98		0.016	
	Ti	4	2.99		0.017	

^a Fit range (*R*) 0.50–3.00 Å.

although more than enough to provide useful information. Figure 7 shows the experimental and best fit k^2 weighted EXAFS for milled and cycled samples. The resulting parameters from the fitting procedure have been summarized in Tables 2 and 3.

Table 2 shows the results of the analysis for the milled M10-org sample as compared to TiO₂ anatase and the Ti-iso reference sample. Good agreement (Figure 7) was obtained confirming that mainly Ti(IV) species are present in the as milled sample (anatase like TiO₂ local structure).

The most interesting analysis, however, is the one summarized in Table 3. Here the cycled samples FT spectra were fitted by considering a mixture of the Ti₂O₃ and TiB₂ phases as major components. Despite the presence of other phases like TiO₂ and TiO cannot be fully disregarded, these components are considered to be negligible in this model according to previous data in Figure 6. The major formation of Ti₂O₃ during first desorption of milled MgH₂ with TiO₂ additives, has been also previously reported by Hanada et al.³¹ on the basis of EXAFS data of the single hydride system. The three peak structure in the 1.1–2.2 Å (no phase shift correction) region is well reproduced with the proposed model. The two peaks at 1.1 and 1.7 Å correspond mainly to Ti–O distances in Ti₂O₃ while the third peak at around 1.9 Å correspond to Ti–B distances in TiB₂. Data in Figure 7 and Table 3 show the progressive reduction of the Ti additive upon desorption from the initial TiO₂ phase to a mixture of Ti₂O₃

TABLE 3: EXAFS Fitting Parameters^a of Ti₂O₃ (Reference), TiB₂ (Reference), and Partially and Fully Desorbed and Absorbed Samples

	shell	<i>N</i>	<i>R</i> (Å)	ΔE (eV)	σ (Å)	<i>R</i> factor
Ti ₂ O ₃ (rhombohedral. R-3ca=5.1580 Å, $c = 13.6111 \text{ \AA}$)	O	3	2.03			
	O	3	2.07			
	Ti	1	2.58			
	Ti	3	2.99			
Ti ₂ O ₃ reference	O	3	2.04	3.51	0.004	0.119
	O	3	2.08		0.005	
	Ti	1	2.59		0.006	
	Ti	3	3.02		0.008	
TiB ₂ (hexagonal. P6/mmm $a = 3.030 \text{ \AA}$, $c = 3.232 \text{ \AA}$)	B	12	2.38			
	Ti	6	3.02			
	B	12	2.36	-0.99	0.005	0.097
	Ti	6	3.03		0.006	
TiB ₂ reference	O	3	2.14	-0.35	0.009	0.022
	O	3	2.14		0.026	
	Ti	1	2.42		0.030	
	Ti	3	3.27		0.045	
M10–1/3des	B	12	2.40	-9.34	0.003	
	Ti	6	3.22		0.022	
	O	3	2.14	0.73	0.008	0.042
	O	3	2.15		0.027	
M10–1/2des	Ti	1	2.56		0.031	
	Ti	3	3.21		0.039	
	B	12	2.37	-9.52	0.003	
	Ti	6	3.12		0.036	
M10-des	O	3	2.17	2.36	0.009	0.037
	O	3	2.18		0.024	
	Ti	1	2.56		0.032	
	Ti	3	3.27		0.037	
M10–1/2abs	B	12	2.38	-8.79	0.005	
	Ti	6	3.05		0.023	
	O	3	2.15	1.61	0.013	0.045
	O	3	2.16		0.027	
M10-abs	Ti	1	2.56		0.033	
	Ti	3	3.23		0.040	
	B	12	2.36	-9.30	0.006	
	Ti	6	3.05		0.028	
M10-abs	O	3	2.15	2.41	0.010	0.037
	O	3	2.17		0.026	
	Ti	1	2.56		0.038	
	Ti	3	3.24		0.047	
48% TiB ₂	B	12	2.36	-9.01	0.005	
	Ti	6	3.04		0.021	

^a Fit range (*R*) 0.50–3.00 Å.

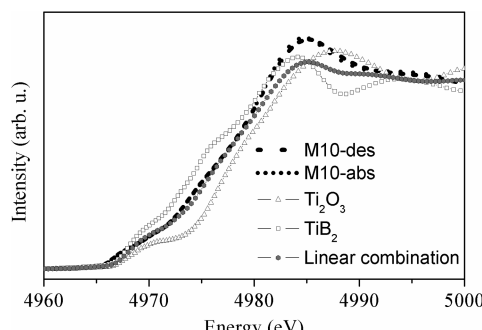


Figure 8. Ti-K edge XANES data for fully desorbed and absorbed samples (with 10 mol % Ti-iso) as compared to reference materials and the linear combination of 1:1 ratio of Ti_2O_3 and TiB_2 .

and TiB_2 that achieve an almost constant molar ratio of 1:1. Main evolution occurs during first 1/2 of desorption. During the rehydrogenation processes changes are less pronounced indicating a decreasing transformation rate toward the TiB_2 state. It confirms that once the active species are formed during first desorption, the oxidation state and local structure of the Ti-based additive remain almost constant.

Additionally we have represented in Figure 8 the result of a linear combination of the XANES spectra in a 1:1 ratio of the two spectra from reference samples Ti_2O_3 and TiB_2 . There is a good agreement of the edge position in this linear combination with the spectra of fully desorbed and absorbed samples, this confirms the data obtained from the EXAFS fitting.

The signal-to-noise ratio for EXAFS data in the samples with 5 mol % Ti-iso additive is less favorable than in samples with 10 mol % Ti-iso. Therefore only the EXAFS analysis for the M10 samples have been shown here. However, preliminary FT curves for the M5 samples clearly evidence that in this case the molar ratio between Ti_2O_3 and TiB_2 phases in the final state is lower than 1:1. Approximate values of 3:7 phase ratio have been obtained. The results support the assumption that a strong source of oxygen in these samples is the Ti-iso additive itself. With smaller amounts of additive a higher proportion of TiB_2 is obtained.

The chemical characterization of the Ti-based additive has been also investigated by XPS in the surface and sub surface

regions. Figure 9a shows the Ti 2p photoelectron peak region for the as prepared M5-org sample as compared to the fully desorbed and fully absorbed samples. The Ti 2p photoelectron spectra from two reference powders such as TiO_2 anatase and TiB_2 have been also included in the figure. The $2p^{3/2}$ and $2p^{1/2}$ peaks at 458.6 and 464.7 eV are typical of fully oxidized Ti(IV), while the small peaks at 454.1 and 460.2 eV are the ones expected for Ti(II) and TiB_2 phase. The TiB_2 commercial reference powder is a heavily oxidized material in the surface region so that only small peaks of the TiB_2 phase are detected along with strong oxide peaks.

For the original milled sample (M5-org), fully oxidized Ti (IV), as the majority phase, is clearly detected on the surface. The shoulders at lower binding energies are attributed to reduced oxides like Ti_2O_3 ³² also present at the surface. No traces of TiB_2 phase formation during milling were observed. A relevant result in Figure 9a is that Ti species are not further detected on the surface upon cycling, indicating a migration of Ti species into the bulk. This result shows that the Ti-boride active phase may play its main role at the bulk LiBH_4 –Mg interface where it is promoting the nucleation of the MgB_2 . The rate limiting processes, related to the observed plateau in volumetric measurements, appears to be, not the hydrogen diffusion from the surface, but the nucleation of the MgB_2 phase to be formed. The high dispersion of the Ti species (Ti-oxide and Ti-boride) at the bulk phase boundaries may additionally limit grain growth of the formed phases, increasing interfacial area and improving the kinetics in both charging and decharging processes.

Figure 9b shows the Ti 2p photoelectron peaks for the same samples as in Figure 9a but after one hour Ar^+ sputtering treatment (spectra from reference samples are included as recorded). The removal of material, by long time sputtering, shows the presence of the Ti phases in the cycled samples in the subsurface region. As shown in sample M5-org, Ar^+ sputtering produces reduction of titanium oxide, which likely is due to preferential sputtering of oxygen.³² Due to this effect, solid conclusions cannot be achieved from XPS regarding the oxidation state of Ti in the bulk of cycled samples. According to Figure 9b, Ti in the fully desorbed sample appears to be more oxidized than in the fully absorbed one. In both cases the small Ti signal appears at different sputtering times so that exposure

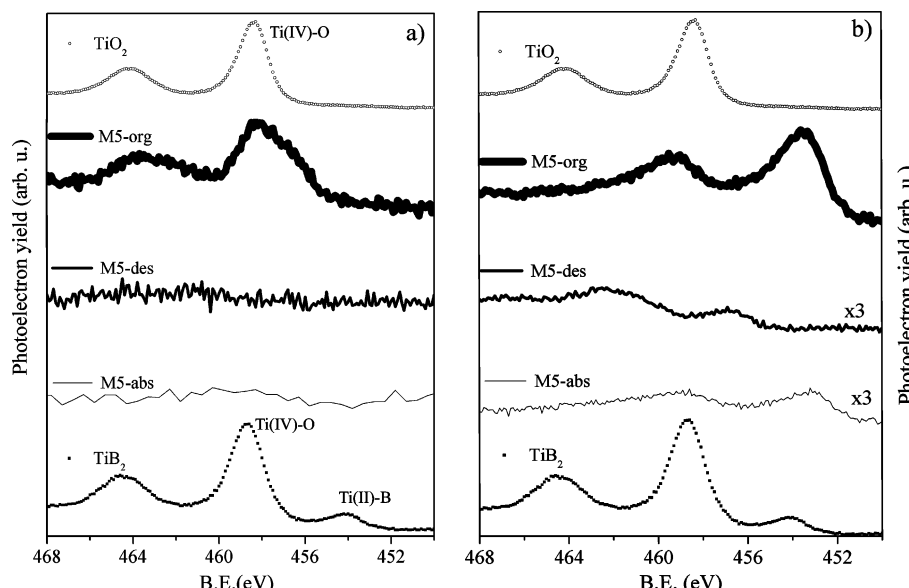


Figure 9. Ti 2p photoemission spectra of M5-org, M5-des and M5-abs before (a) and after (b) 1 h Ar^+ sputtering compared to the references TiO_2 and TiB_2 .

to Ar⁺ sputtering is not equivalent. Nevertheless, the migration of Ti species from the surface to the bulk during the first desorption is the main effect to be concluded from the XPS experiments.

Conclusions

The Ti-isopropoxide additive has a significant influence on the sorption kinetics of the 2LiBH₄ + MgH₂ reactive hydride composite. Under the experimental conditions presented in this work, the dehydrogenation process shows two steps: First desorption from MgH₂ and second desorption from LiBH₄ coupled to the formation of MgB₂. In the present study, the evolution of chemical state and local structure of the Ti-based additives were investigated by XANES, EXAFS, and XPS. For the first time these techniques have been reported for the study of Ti-based additives in the RHC systems. They have been shown to be very valuable for the characterization of the highly dispersed amorphous or nanocrystalline particles formed by the Ti additive.

The as prepared RHC sample after ball milling shows a fully oxidized Ti(IV) phase, most likely TiO₂ anatase. During first desorption reduced Ti-oxide (Ti₂O₃) and TiB₂ phases are formed remaining stable during further cycling treatments. Main evolution occurs during first 1/2 of desorption. The progressive reduction of the Ti additive upon desorption from the initial TiO₂ phase to a mixture of mainly Ti₂O₃ and TiB₂ finally achieve an almost constant molar ratio of 1:1 for a 10 mol % Ti-iso additive addition. During the rehydrogenation processes changes are less important confirming that once the active species are formed during first desorption, the oxidation state and local structure of the Ti-based additive remains almost constant. The local structure formed after ball milling or dehydrogenation/rehydrogenation is close to that of corresponding oxides and borides but in a more disarrangement state. The reduction process and the formation of the TiB₂ phase are coupled with the migration of Ti-species from the surface to the bulk of the material as determined by XPS.

Initial explanations are suggested on how the reduced Ti-oxide and Ti-boride active species can improve the reaction kinetics. In one hand, highly dispersed TiB₂ nanoparticles could improve the heterogeneous nucleation of the MgB₂ thus reducing the delay between the MgH₂ and the LiBH₄ desorption by favoring desorption from the borohydride at the LiBH₄/Mg interface. On the other hand grain refinement effects have been also proposed as a possible mechanism for kinetic improvement in this system due to the presence of highly dispersed titanium oxides and borides at the grain boundaries. A good distribution and a sufficient amount of the nucleation agents are mandatory for efficient heterogeneous nucleation. Ti-isopropoxide favors additive dispersion.

Further studies are still needed to fully understand the role of additives and reaction mechanism in the very promising RHC systems.

Acknowledgment. Financial support by the Marie Curie Program (MRTN-CT-2006-035366) as well as the Spanish MICINN (CTQ2009-13440) and the Junta de Andalucía are

acknowledged. XAS facilities at BM29 in ESRF and the help of Dariusz A. Zajac at E4 in DESY are gratefully acknowledged.

References and Notes

- (1) Fichtner, M. *Adv. Eng. Mater.* **2005**, 6, 433.
- (2) Schlapbach, L.; Züttel, A. *Nature* **2001**, 414, 353.
- (3) Dornheim, M.; Eigen, N.; Bakhordarian, G.; Klassen, T.; Bormann, R. *Adv. Eng. Mater.* **2006**, 8, 377.
- (4) Fujii, H.; Ichikawa, T. *Physica B* **2006**, 383, 45.
- (5) Züttel, A.; Borgschulte, A.; Orimo, S.-I. *Scripta Mater.* **2007**, 56, 823.
- (6) Schüth, F.; Bogdanovic, B.; Felderhoff, M. *Chem. Commun.* **2004**, 2249.
- (7) Friedrichs, O.; Borgschulte, A.; Kato, S.; Buchter, F.; Gremaud, R.; Remhof, A.; Züttel, A. *Chem.—Eur. J.* **2009**, 15, 5531.
- (8) Züttel, A.; Renth, S.; Fischer, P.; Wenger, P.; Sudan, P.; Mauron, Ph.; Emmenegger, Ch. *J. Alloys Compd.* **2003**, 356–357, 515.
- (9) Vajo, J. J.; Skeith, S. L.; Mertens, F. *Phys. Chem. Lett. B* **2005**, 109, 3719.
- (10) Bakhordarian, G.; Klassen, T.; Dornheim, M.; Bormann, R. *J. Alloys Compd.* **2007**, 440, L18.
- (11) Orimo, S.; Nakamori, Y.; Kitahara, G.; Miwa, K.; Ohba, N.; Towata, S.; Züttel, A. *J. Alloys Compd.* **2005**, 404–406, 427.
- (12) Mauron, P.; Butcher, F.; Friedrichs, O.; Remhof, A.; Bielmann, M.; Zwicky, C. N.; Züttel, A. *J. Phys. Chem. B* **2008**, 112, 906.
- (13) Friedrichs, O.; Buchter, F.; Borgschulte, A.; Remhof, A.; Zwicky, C. N.; Mauron, Ph.; Bielmann, M.; Züttel, A. *Acta Materialia* **2008**, 56, 949.
- (14) Bösenberg, U.; Doppiu, S.; Mosegaard, L.; Bakhordarian, G.; Eigen, N.; Borgschulte, A.; Jensen, T.; Cerenius, Y.; Gutfleisch, O.; Klassen, T.; Dornheim, M.; Bormann, R. *Acta Mater.* **2007**, 55, 3951.
- (15) Vajo, J. J.; Salguero, T. T.; Gross, A. F.; Skeith, S. L.; Olson, G. L. *J. Alloys Compd.* **2007**, 446–447, 409.
- (16) Fan, M.-Q.; Sun, L.-X.; Zhang, Y.; Xu, F.; Zhang, J.; Chu, H.-L. *Int. J. Hydrogen Energy* **2008**, 33, 74.
- (17) Bakhordarian, G.; Jensen, T. R.; Doppiu, S.; Bösenberg, U.; Borgschulte, A.; Gremaud, R.; Cerenius, Y.; Dornheim, M.; Klassen, T.; Bormann, R. *J. Phys. Chem. C* **2008**, 112, 2743.
- (18) Friedrichs, O.; Martínez-Martínez, D.; Guilera, G.; Sánchez López, J. C.; Fernández, A. *J. Phys. Chem. C* **2007**, 111, 10700.
- (19) Friedrichs, O.; Sánchez López, J. C.; López-Cartes, C.; Klassen, T.; Bormann, R.; Fernández, A. *J. Phys. Chem. B* **2006**, 110, 7845.
- (20) Friedrichs, O.; Auguey-Zinsou, F.; Ares Fernández, J. R.; Sánchez López, J. C.; Justo, A.; Klassen, T.; Bormann, R.; Fernández, A. *Acta Mater.* **2006**, 54, 105.
- (21) Bösenberg, U.; Vainio, U.; Pranzas, P. K.; Bellotta von Colbe, J. M.; Goerigk, G.; Welter, E.; Dornheim, M.; Schreyer, A.; Bormann, R. *Nanotechnology* **2009**, 20, 204003.
- (22) Ignatov, A. Yu. Graetz, J. Chaudhuri, S. Salguero, T. T. Vajo, J. J. Meyer, M. S. Pinkerton, F. E. Tyson. T. A. *Spatial Configurations of Ti- and Ni- Species Catalyzing Complex Metal Hydrides: X-Ray Absorption Studies and First-Principles DFT and MD Calculations*"; 13th International Conference on X-Ray Absorption Fine Structure (XAFS13), 2007, Standford, CA.
- (23) Filippini, A.; Borowski, M.; Bowron, D. T.; Ansell, S.; Di Cicco, S.; De Panfilis, S.; Itié, J.-P. *Rev. Sci. Instrum.* **2000**, 71, 2422.
- (24) Ravel, B.; Newville, M. *J. Synchrotron Radiat.* **2005**, 12, 537.
- (25) Newville, M. *J. Synchrotron Radiat.* **2001**, 8, 322.
- (26) Rehr, J. J.; Albers, R. C. *Rev. Mod. Phys.* **2000**, 72, 621.
- (27) Terabe, K.; Kato, K.; Yamaguchi, S.; Imai, A.; Iguchi, Y. *J. Mater. Sci.* **1994**, 29, 1617.
- (28) Diré, S.; Babonneau, F. *J. Sol-Gel Sci. Technol.* **1994**, 2, 139.
- (29) Wang, Y.; Wang, H. Y.; yang, Y. F.; Jiang, Q. C. *Mater. Sci. Eng. A* **2008**, 478, 9.
- (30) Qiu, D.; Zhang, M. X.; Fu, H. M.; Kelly, P. M.; Taylor, J. A. *Philos. Mag. Lett.* **2007**, 87, 505.
- (31) Hanada, N.; Ichikawa, T.; Isobe, S.; Nakagawa, T.; Tokoyoda, K.; Honma, T.; Fuji, H.; Kojima, Y. *J. Phys. Chem. C* **2009**, 113, 13450.
- (32) Soriano, L.; Abbate, M.; Vogel, J.; Fuggle, J. C.; Fernández, A.; González-Felipe, A. R.; Sacchi, M.; Sanz, J. M. *Surf. Sci.* **1993**, 290, 427.